JACS JOURNAL OF THE AMERICAN CHEMICAL SOCIETY
Article
pubs.acs.org/JACS

Site-Specific Transition Metal Occupation in Multicomponent Pyrophosphate for Improved Electrochemical and Thermal Properties in Lithium Battery Cathodes: A Combined Experimental and Theoretical Study

Rana. A. Shakoor,[†,¶] Heejin Kim,[‡,¶] Woosuk Cho,[⊥] Soo Yeon Lim,[‡] Hannah Song,[∥] Jung Woo Lee,[†,§] Jeung Ku Kang,[†,‡,§] Yong-Tae Kim,[∥] Yousung Jung,*[,‡,§] and Jang Wook Choi*[,‡,§]

[†]Department of Materials Science and Engineering, [‡]Graduate School of EEWS (WCU), and [§]KAIST Institute nanoCentury, Korea Advanced Institute of Science and Technology (KAIST), Yuseong-gu, Daejeon 305-701, Republic of Korea

[⊥]Advanced Batteries Research Center, Korera Electronics Technology Institute (KETI), Bundang-gu, Seongnam-si, Gyeonggi-do 463-816, Republic of Korea

[∥]Energy System Major, School of Mechanical Engineering, Pusan National University, Geumjeong-gu, Busan 609-735, Republic of Korea

Supporting Information

ABSTRACT: As an attempt to develop lithium ion batteries with excellent performance, which is desirable for a variety of applications including mobile electronics, electrical vehicles, and utility grids, the battery community has continuously pursued cathode materials that function at higher potentials with efficient kinetics for lithium insertion and extraction. By employing both experimental and theoretical tools, herein we report multicomponent pyrophosphate ($Li_2MP_2O_7$, M = $Fe_{1/3}Mn_{1/3}Co_{1/3}$) cathode materials with novel and advantageous properties as compared to the single-component analogues and other multicomponent polyanions. $Li_2Fe_{1/3}Mn_{1/3}Co_{1/3}P_2O_7$ is formed on the basis of a solid solution among the three individual transition-metal-based pyrophosphates. The unique crystal structure of pyrophosphate and the first principles calculations show that different transition metals have a tendency to preferentially occupy either octahedral or pyramidal sites, and this site-specific transition metal occupation leads to significant improvements in various battery properties: a single-phase mode for Li insertion/extraction, improved cell potentials for Fe^{2+}/Fe^{3+} (raised by 0.18 eV) and Co^{2+}/Co^{3+} (lowered by 0.26 eV), and increased activity for Mn^{2+}/Mn^{3+} with significantly reduced overpotential. We reveal that the favorable energy of transition metal mixing and the sequential redox reaction for each TM element with a sufficient redox gap is the underlying physical reason for the preferential single-phase mode of Li intercalation/deintercalation reaction in pyrophosphate, a general concept that can be applied to other multicomponent systems. Furthermore, an extremely small volume change of ~0.7% between the fully charged and discharged states and the significantly enhanced thermal stability are observed for the present material, the effects unseen in previous multicomponent battery materials.

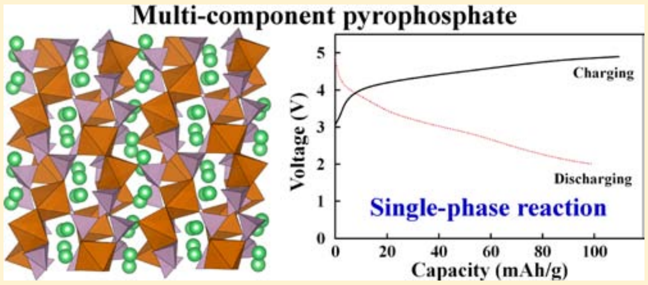

■ INTRODUCTION

So far lithium-ion batteries (LIBs) have been successful in empowering various portable electronics. Beyond these small applications, various energy and environmental issues are currently leading to the expansion of the LIB territory into larger-scale applications including electrified vehicles and utility power grids.[1] Clearly, these large-scale applications impose more challenging standards in various aspects including energy/power densities, lifetime, cost, and safety. This situation has driven the battery community to pursue cathode materials that hold higher energy densities or facilitate more efficient kinetics for Li insertion/extraction. The most representative efforts along these directions are the exploration of crystal structures based on diverse polyanions (fluorophosphate,[2,3] fluorosulfate,[4−9] borate,[10,11] pyrophosphate,[12−14] silicate,[15,16] etc.), the substitution of transition metals (TMs) to raise the operation voltage, and the activation of single-phase Li insertion/extraction. Interestingly, these material manipulations frequently arise together, giving synergistic effects on electrochemical properties.

As a Li insertion/extraction mechanism in active materials, the single-phase process has been intensively studied because of its favorable kinetics for charge−discharge processes.[17−19]

Received: May 2, 2012
Published: June 21, 2012

dx.doi.org/10.1021/ja3042228 | J. Am. Chem. Soc. 2012, 134, 11740−11748

Compared to the two-phase process in which the nucleation and growth of the second phase occur in the presence of concrete phase boundaries, the single-phase process contains a lower kinetic barrier to overcome for Li ion diffusion and has been thus considered as a more desirable mechanism for high power cell operations. While various underlying origins including a decrease in the energy of mixing,[20] super exchange interaction of TMs with oxygen,[21] and structural defects and cation vacancies[22] have been suggested, the most viable experimental methods to trigger the single-phase mode are in nanosizing the active materials,[22] increasing the operation temperature,[17] and implementing more than one TM, namely, multicomponent TMs.[5,10,23,24] Moreover, beyond the activation of the single-phase behavior, the multicomponent TMs could also tune the operation voltage toward higher energy densities. The multicomponent olivine materials, i.e., $LiMPO_4$ (M = multicomponent TMs),[20,21,23−26] are good examples and have been indeed profoundly studied.[27] These compounds exhibit higher cell potentials compared to those of pure Fe-based counterparts.

Among various polyanion-based compounds, recently, pyrophosphates ($Li_2MP_2O_7$, M = Fe, Mn, Co) have received considerable attention[12−14] after the Barker group's prediction that they can be used as cathode materials.[28] The Whittingham group first measured the electrochemical behavior of pyrophosphate,[29] and the Yamada group[14] reported a discharge capacity of ∼120 mAh g^{-1} for the case of M = Fe with a redox potential around 3.5 V vs Li/Li^+. The Whittingham group expanded to M = $Fe_x Mn_{1-x}$ ($0 \leq x \leq 1$) to raise the operation potential,[13] but it turned out that the addition of Mn significantly decreases the specific capacity. The Kang group[12] also examined the M = Co case and found that Co pyrophosphate exhibits a specific capacity of ∼85 mAh g^{-1} with an average voltage of ∼5.0 V, which is too high for stable operations of typical LIB electrolytes. As an attempt to improve the electrochemical properties of this pyrophosphate family, and simultaneously inspired by the multicomponent effect on the favorable Li insertion/extraction mode as well as operation potential, in this study, we investigate a multicomponent pyrophosphate ($Li_2Fe_{1/3}Mn_{1/3}Co_{1/3}P_2O_7$). Unlike the M = Fe_xMn_{1-x} case, the multicomponent system based on these three TMs raise the cell potential without sacrificing the capacity much. In fact, the specific capacity indicates that all of the TMs including Mn and Co are active. Moreover, the multicomponent TMs activate a single-phase mode for Li insertion/extraction with a very small volume change of 0.7% between the fully charged and discharged states. By employing first principles calculations, we found that, contrary to the multicomponent olivine where all of the TMs occupy equivalent octahedral sites, the crystal structure of multicomponent pyrophosphate allows each TM to distinctively occupy either octahedral or pyramidal sites. This TM-dependent structural configuration, we suggest, plays a key role for the single-phase behavior, the anomalously small volume change, and other unique electrochemical properties. Furthermore, the multicomponent system contributes to excellent thermal stability of the compound, suggesting good safety of this compound for practical applications.

■ RESULTS

Crystal Structure and Solid Solution. $Li_2Fe_{1/3}Mn_{1/3}Co_{1/3}P_2O_7$ was synthesized through a simple and commercially viable solid-state reaction process. The compound was prepared by reacting stoichiometric amounts of lithium carbonate (Li_2CO_3), ammonium phosphate dibasic ($(NH_4)_2HPO_4$), and metal oxalate ($MC_2O_4 \cdot H_2O$, M = Fe, Mn, Co) at 600 °C for 6 h under argon flow. More detailed synthetic procedures are described in the Supporting Information. The elemental composition of the as-synthesized material was characterized by inductively coupled plasma mass spectrometry (ICP-MS), and the data are presented in Table S1 in the Supporting Information. The data confirm the formation of the compound with the designated stoichiometry. The ICP data for the electrochemically delithiated phase are also shown in the same table. In addition, FT-IR analyses also support the formation of the pyrophosphate compound (Figure S1). Symmetric vibrations of P−O−P bonds at ∼750 and 950 cm^{-1} indicate the presence of the pyrophosphate group in this material. The O−P−O and P−O vibrations can be attributed to PO_3 bonds in $(P_2O_7)^{4-}$, which is consistent with previous reports.[12,30,31]

Figure 1 shows the crystal structure of $Li_2MP_2O_7$ (M = Fe, Mn, Co) viewed along the *b*-axis. $Li_2Fe_{1/3}Mn_{1/3}Co_{1/3}P_2O_7$ is isostructured with $Li_2MnP_2O_7$,[14,32] $Li_2FeP_2O_7$,[12−14] and $Li_2CoP_2O_7$,[12] with all holding monoclinic symmetries that belong to the space group $P2_1/c$. The most distinctive feature of pyrophosphates compared to the other structures (olivine, spinel, or layered) is that the two TM sites are in different environments, octahedral (Oc) and distorted square pyramidal (Py) coordinations. For the perfect structure, as in the case of M = Mn,[32] the TM and Li occupy two and four different crystallographic sites, respectively, as illustrated in Figure 1a. On the other hand, the Fe- and Co-based pyrophosphates have a partial site exchange between the TMs at Py sites and lithium at Li1 sites by an amount of ∼30%, leading to three TM sites and five Li sites.[12] This site exchange ratio can be measured from the relative intensity between the (−111) and (200) X-ray diffraction (XRD) peaks at around 15°. The higher intensity of the (−111) peak compared to that of the (200) peak indicates a higher degree of site exchange.[12] The XRD data (Figure 2) indicate that our multicomponent compound has a smaller degree of site exchange compared to those of the Fe or Co single-component compounds, which will be discussed later. The correlations of the 2θ-crystal plane and the lattice

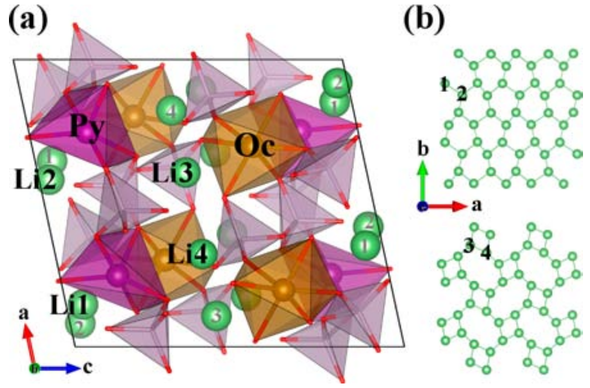

Figure 1. (a) Crystal structure of pyrophosphate projected along the *b*-axis presents two crystallographic metal sites, octahedral (Oc) and pyramidal (Py), and four lithium sites (Li1−Li4). (b) Lithium sites Li1 and Li2 are in the same layer, and lithium sites Li3 and Li4 are in the other layer. Both lithium layers have two-dimensional diffusion pathways along the *ab* plane.

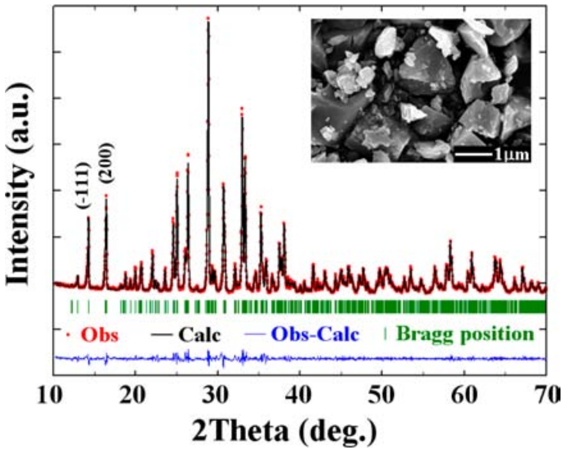

Figure 2. Peak-matched XRD spectrum of multicomponent pyrophosphate. The inset SEM image shows the size and morphology of the as-synthesized powder particles.

parameters are tabulated in Tables S2 and S3, respectively. The lattice parameters of other reported members in the pyrophosphate family are also presented for comparison. Overall, the peak locations as well as the estimated lattice parameters are consistent with previous reports, which confirm that the synthesized multicomponent compound is highly crystalline with a pure phase. Moreover, the lattice parameters are comparable to the average values of $Li_2FeP_2O_7$, $Li_2MnP_2O_7$, and $Li_2CoP_2O_7$, thus providing the first indication that all of the three components are homogeneously mixed (solid solution) without phase segregation. Considering that the particle sizes of the as-synthesized compound are 1−2 μm (Figure 2 inset), the solid-solution formation in this multicomponent system implies that the homogeneous mixing among the three TMs during the synthesis is thermodynamically favorable.

Electrochemical Properties and Volume Change. Electrochemical properties of $Li_2Fe_{1/3}Mn_{1/3}Co_{1/3}P_2O_7$ were characterized by preparing coin-type half cells in which Li foil was used as both the reference and counter electrodes. One molar lithium hexafluorophosphate ($LiPF_6$) in ethylene carbonate (EC) diethylene carbonate (DEC) (1:1 in volume) and polyethylene separators (Celgard 2400) were used as electrolyte and separators, respectively. More detailed cell preparation procedures are described in the Supporting Information. Before the electrochemical testing, the synthesized material was carbon-coated to improve the electrical conductivity. Annealing was carried out after the carbon coating to restore the original crystallinity of the material. The comparison of XRD spectra before and after the carbon-coating (Figure S2) indicates that the carbon-coating process and subsequent annealing treatment do not result in the formation of any secondary phase. The galvanostatic intermittent titration technique (GITT) and its Quasi-open circuit potential (QOCP) data measured at a C/20 rate are presented in Figure 3. The clear single-phase Li insertion/extraction is observed and is verified consistently by both *ex situ* and *in situ* X-ray diffraction (XRD) measurements. *Ex situ* data over the entire 2θ range, zoomed-in data in the smaller θ range, and *in situ* data are presented in Figure 4, and Figures S3 and S4, respectively. As indicated by these data, throughout charging and discharging processes, the shifts of peak positions for all of the crystal planes are almost negligible and no secondary phase is formed. During delithiation, most peaks including those corresponding to (−111), (200), and (−202) planes are shifted to higher 2θ values, which indicates a decrease in the lattice distances along those planes. Lattice parameters and unit cell volumes were obtained at different voltages during charging and discharging using FullProf software[33] (Figure 5 and Table S4). As shown in Figure 5, during delithiation, lattice parameters in all of the *a*-, *b*-, and *c*-axes and thus unit cell

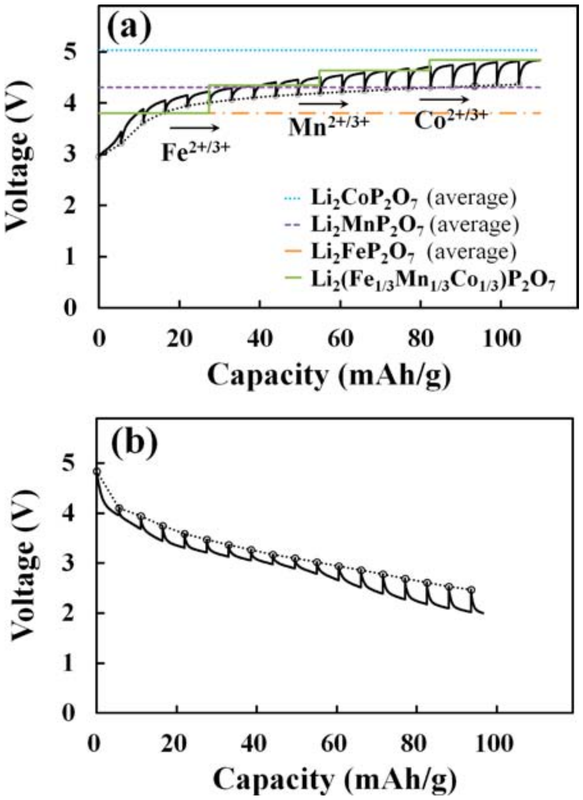

Figure 3. (a) QOCP profile measured at a C/20 rate for charging. The dashed lines in color (blue, purple, and orange) are the calculated average voltages for each of the single-component compounds. An approximately calculated potential profile for the multicomponent compound is shown with a green solid line. The first 1/3 of the capacity is attributed to the $Fe^{2+/3+}$ redox couple, and the next 1/3 and the last 1/3 of the capacity are attributed to the $Mn^{2+/3+}$ and $Co^{2+/3+}$ redox couples, respectively. (b) A QOCP profile for discharging. All the voltages in this Figure are with respect to Li/Li^+.

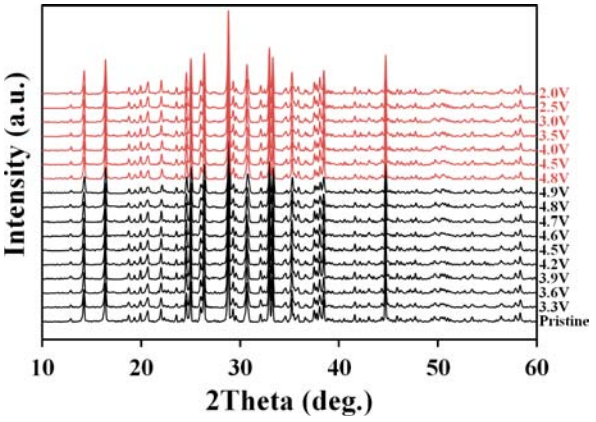

Figure 4. *Ex situ* XRD measurements for charging (black) and discharging (red) processes at denoted potentials. Clear single-phase reactions are observed throughout the entire range of a full cycle.

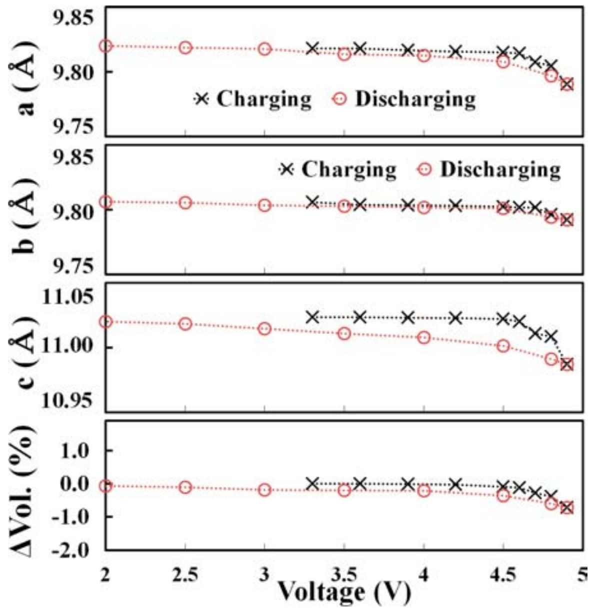

Figure 5. Lattice parameters and unit cell volume changes as a function of voltage. These values were obtained from the *ex situ* XRD analyses performed during charging and discharging within a voltage window of 2.0−4.9 V vs Li/Li$^+$.

volumes successively decrease. In contrast, these values increase and recover to the original values during lithiation, which indicates the reversible character of the crystal structure during a full cycle. The most striking result with regard to these lattice parameters is the exceptionally small volume change during charging and discharging: The volume difference at the end of charging and discharging is only 0.7%. In addition, the concentrated volume change at the end of the voltage region during the charge (Figure 5c) is associated with the charging profile in which a large portion of the capacity is given in that voltage region. This value is remarkably smaller than those of other cathode materials based on two-phase reactions: $LiFePO_4$ (6.5%),[34] $LiMnPO_4$ (9.0%),[35] spinel structures $LiMn_2O_4$ (6.4%),[36] and fluorosulphates $LiFeSO_4F$ (10%).[6] This value is comparable to the $Li(Fe_{1-\delta}Mn_{\delta})SO_4F$ case[5] that shows the smallest value (0.6%) ever reported. The extremely small volume change should be related to the single-phase reaction during Li insertion/extraction that contributes to preserving the overall crystal structure while maintaining a very small miscibility gap between the charged and discharged states.[37] Importantly, it is noteworthy that the minimal volume change must be beneficial for robust battery performance because it involves negligible distortion of crystal structures. This volume change value was reproducible over multiple samples and XRD runs.

Despite these attractive properties, there is some room for improvementwith regard to cycling and rate performance. After 35 cycles, ~80% of the initial capacity is retained (Figure 6a), and ~50% of the capacity is retained as the c-rate increases from C/20 to 2C (Figure 6b). The Coulombic efficiencies during the cycling test are around 91%. While these values are similar to those of the Fe-based pyrophosphate,[14] the relatively lower efficiencies compared to those of other cathode materials are likely attributed to Li trapping that originates from Li-TM antisite defects. In particular, it is anticipated that Li at Li1 and Li2 sites (Figure 1b) suffers more from the Li trapping than those at other sites because those two sites are known to be vulnerable to the antisite defects.[12] Nonetheless, the rate performance of the multicomponent pyrophosphate is clearly superior to that of the pure Fe-based pyrophosphate,[14] still verifying the advantages of the single-phase reaction with the minimal volume change over the two-phase reaction with a larger volume change. The pure Fe pyrophosphate exhibits flat plateaus[14] with a volume difference of 1.8% (Figure S5). The moderate cycling and rate performance of the pyrophosphate family are seemingly due to the low electric conductivity and are expected to be addressed by nanosizing.

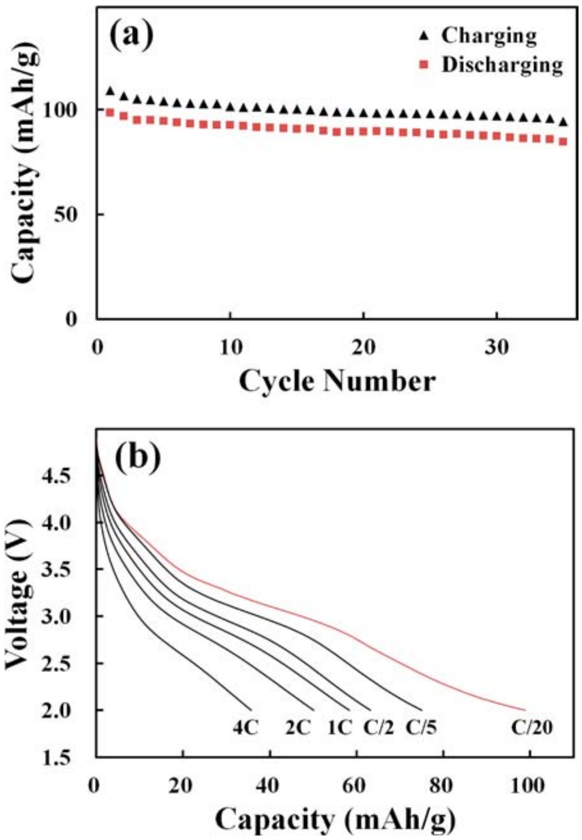

Figure 6. (a) Cycling performance and (b) rate capability of $Li_2Fe_{1/3}Mn_{1/3}Co_{1/3}P_2O_7$. Voltages are with respect to Li/Li$^+$. For the cycling test, the c-rate is C/20 for both charge and discharge. For the rate capability test, the charging rate is C/20. The mass loading of the active material is 1.45 mg cm^{-2} in both (a) and (b).

Thermal Stability. Thermal stability of $Li_2Fe_{1/3}Mn_{1/3}Co_{1/3}P_2O_7$ was also tested as thermal stability of cathode materials is critical for cell safety. For this characterization, thermogravimetric analysis (TGA) and differential thermal analysis (DTA) were first performed for both pristine ($Li_2Fe_{1/3}Mn_{1/3}Co_{1/3}P_2O_7$) and partially delithiated ($LiFe_{1/3}Mn_{1/3}Co_{1/3}P_2O_7$) samples, and their data are presented in Figure S6 and Figure 7, respectively. In both measurements, temperature was scanned from room temperature to 550 °C at a rate of 10 °C/min under argon atmosphere. The TGA data indicate that the partially delithiated one exhibits a negligible weight loss (~2%) in the given temperature range. The DTA profile also shows the stable thermal property of the partially delithiated compound as it does not show any exo/endothermic peaks. TGA/DTA data of the pristine compound displays the similar behavior, again supporting the thermal stability of $Li_2Fe_{1/3}Mn_{1/3}Co_{1/3}P_2O_7$. More interestingly, this thermal stability of $Li_2Fe_{1/3}Mn_{1/3}Co_{1/3}P_2O_7$ is conspicuously

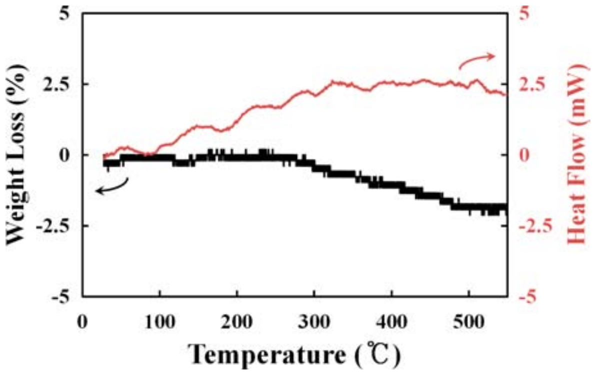

Figure 7. TGA (black) and DTA (red) data for the delithiated state ($Li_1Fe_{1/3}Mn_{1/3}Co_{1/3}P_2O_7$).

better than that of $Li_2FeP_2O_7$: In the case of $Li_2FeP_2O_7$, the delithiated one shows a high exothermic peak at ~500 °C and more significant weight loss (~5%), confirming its instability above 500 °C.[12] While the underlying mechanism for the enhanced thermal stability is not trivial to grasp, we expect that the multicomponent solid-solution formation also plays a role.

Impressed by the excellent thermal behavior of the multicomponent pyrophosphate, we performed *in situ* XRD characterization at various temperatures in the temperature range of 25−550 °C to verify the stability of the crystal structure. See the Supporting Information for detailed procedures. This characterization was also done for both the pristine (Figure S6) and the partially delithiated (Figure 8). As shown in Figure 8, the delithiated phase does not show any additional peak in the entire temperature range. There is only peak shifting toward lower 2θ values, which can be interpreted as the unit cell expansion originating from thermal vibrations of the lattice upon heating. The pristine compound also behaves similarly to the partially delithiated one (Figure S6). The similar thermal behaviors between the pristine and the partially delithiated also support the complete single-phase character of this compound during Li insertion/extraction. The lattice parameters and unit cell volume for the partially delithiated phase as a function of temperature are presented in Table S5. The thermal stability of the multicomponent pyrophosphate, in fact, is superior to that of other cathode materials including the olivine family that is known to be thermally stable due to the P−O bonding.[38,39] In the pristine phases, $LiMnPO_4$[40] and $LiFePO_4$[41] were reported to be thermally stable up to 400 °C. For the delithiated phases, the thermal stability of the multicomponent pyrophosphate is substantially better than those of $MnPO_4$[42] (150−200 °C) and $CoPO_4$[43] (~250 °C) and is comparable to that of $FePO_4$[17] (~500 °C). These findings may suggest that the thermal behavior of materials can be significantly improved by the solid-solution formation of different TM components. While it is anticipated that both the unique crystal structure and the multicomponent solid-solution formation play a role in leading to the excellent thermal stability, more detailed discussion will be covered in forthcoming papers.

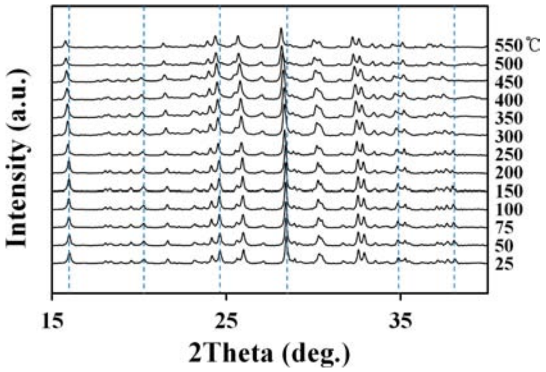

Figure 8. *In situ* XRD data for the delithiated state ($LiFe_{1/3}Mn_{1/3}Co_{1/3}P_2O_7$) measured at various temperatures.

■ DISCUSSION

We performed density functional theory (DFT) calculations using VASP to gain more insights into the origin of solid-solution formation,[44−52] asymmetric shifts of the redox potential for every TM element to be active within the stable electrolyte window, and a mechanism for the single-phase reaction in $Li_2Fe_{1/3}Mn_{1/3}Co_{1/3}P_2O_7$. Computational details are described in Supporting Information.

Energy of Mixing and Site Exchange. The energy of binary mixing (ΔE_2) was first calculated for the TM pairs in which one TM is assigned to the octahedral site and the other TM is to the neighboring pyramidal site. ΔE_n denotes an energy of mixing for n components. If ΔE_n is negative, homogeneous mixing among the TMs is energetically favorable, enabling the formation of solid solution, whereas if ΔE_n is positive, phase separation of the TMs would be preferred. There are six unique binary pairs for a three-component system including Fe, Mn, and Co. As the results are summarized in Table 1, among the six possibilities, only three pairs (Oc, Py) = (Fe, Mn), (Co, Mn), (Co, Fe) yield negative ΔE_2. It is noteworthy that, for all stable pairs with negative ΔE_2, Mn is shown to occupy pyramidal sites, whereas Co tends to occupy octahedral sites consistently. This is in agreement with a previous report that Mn^{2+} is more likely to be in the square pyramidal sites than Fe^{2+} or Co^{2+}.[53] Using the relative energies and Boltzman probabilities of 22 mixed configurations for all binary compounds considered here (Figure S7), we estimated the average octahedral occupancy for each TM in Table 1. The propensity to occupy the octahedral sites is in the order of Co > Fe > Mn, consistent with the binary mixing energy (ΔE_2) results. Thus, we assumed that the experimental structure of the homogeneously mixed $Li_2Fe_{1/3}Mn_{1/3}Co_{1/3}P_2O_7$ is mostly based on the aforementioned 3 stable TM pairs with negative binary mixing energies. To test this assumption, we compared the energy of ternary mixing (ΔE_3) calculated using eq 1 for two

Table 1. Calculated Energy of Binary Mixing (ΔE_2) for Each Pair of Transition Metals in $Li_2A_{0.5}B_{0.5}P_2O_7$ (A and B = Mn, Fe, Co)[a]

octahedral	pyramidal	ΔE_2 (meV)	octahedral occupation
Fe	Mn	−98.1	Fe, 0.82
Mn	Fe	61.9	Mn, 0.18
Co	Mn	−65.6	Co, 0.87
Mn	Co	66.4	Mn, 0.13
Co	Fe	−2.8	Co, 0.57
Fe	Co	19.2	Fe, 0.43

[a] Negative ΔE_2 indicates that the mixing among the TMs is energetically favorable. The last column indicates the calculated average occupancy of the octahedral site for each TM in binary compounds (see also Figure S7 for details).

sets of configurations, one set consisting of stable pairs with negative ΔE_2 and the other set composed of randomly arranged configurations.[21]

$$\Delta E_3 = E(\mathrm{Li_2Fe_{1/3}Mn_{1/3}Co_{1/3}P_2O_7}) - 1/3[E(\mathrm{Li_2FeP_2O_7}) + E(\mathrm{Li_2MnP_2O_7}) + E(\mathrm{Li_2CoP_2O_7})] \quad (1)$$

Ternary configurations constructed based on the stable pairs with negative ΔE_2 indeed give greater negative energies of mixing, ΔE_3, than those created completely randomly. Therefore, the crystal structure of $\mathrm{Li_2Fe_{1/3}Mn_{1/3}Co_{1/3}P_2O_7}$ can be viewed as a homogeneous mixture of stable TM pairs, (Oc, Py) = (Fe, Mn), (Co, Mn), (Co, Fe). Detailed calculation procedures and the configurations considered are described in the Supporting Information.

As a result of these preferential binary mixings of TM pairs, the site exchange between TM and Li in multicomponent systems can be expected to be less significant than those for the Fe or Co single-component counterparts. A previous neutron diffraction experiment showed that Fe- or Co-based pyrophosphates have a partial site exchange between TM at pyramidal sites and lithium at Li1 sites by 30%, whereas Mn at neither pyramidal nor octahedral sites exhibited site exchange.[12] Since Mn occupies 2/3 of the pyramidal sites in $\mathrm{Li_2Fe_{1/3}Mn_{1/3}Co_{1/3}P_2O_7}$, the previous experimental estimation[12] suggests that roughly 10% of TMs in our multicomponent system can be expected to undergo the site exchange with Li ions, as compared to 30% in the single-component pyrophosphates. These site exchanges can be understood by considering the relative stability of various TMs and lithium in pyramidal sites. The calculated site exchange energies shown in Table S6 indeed are consistent with the experimentally observed trend.

Calculated Redox Potentials. The calculated redox potentials of each TM at both Oc and Py sites in the single-component vs multicomponent environments are summarized in Figure 9. The overall potentials are calculated to be in the order of Fe(Oc) < Fe(Py) < Mn(Oc) < Mn(Py) < Co(Oc) < Co(Py) for each $M^{2+/3+}$ redox couple, consistent with the change of net magnetic moments of TMs as a function of delithiation shown in Figures S8 and S9. These computational results suggest that the observed oxidation sequence depends primarily on the identity of TM elements (Fe < Mn < Co) and secondarily on the type of sites (Oc < Py). The calculated potential of ternary system is overestimated compared to the QOCP results (Figure 3a); however, the single phase reaction and voltage shifts are successfully reproduced. From this oxidation sequence and the QOCP data shown in Figure 3, several important advantageous multicomponent effects can be discussed below.

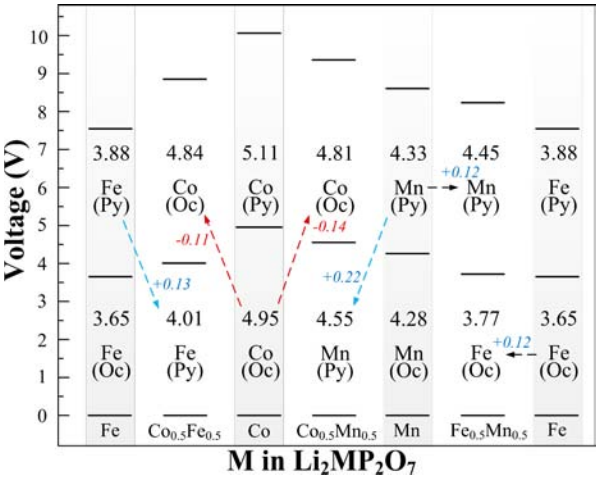

Figure 9. Calculated voltages for octahedral (Oc) and pyramidal (Py) metal sites (M = Fe, Mn, Co) for single- vs binary-component compounds. The change of the redox potential in the multicomponent system depends primarily on the identity of the TM elements (Fe, Mn, Co) but also on the type of sites (Oc, Py).

Measured Capacity. A reversible capacity of ~95 mAh g^{-1} was obtained at C/20 in the first cycle, which suggests that ~0.9 lithium participates in the reaction for each $\mathrm{Li_2Fe_{1/3}Mn_{1/3}Co_{1/3}P_2O_7}$. For reference, the theoretical capacity for one Li reaction per each $\mathrm{Li_2Fe_{1/3}Mn_{1/3}Co_{1/3}P_2O_7}$ is 110 mAh g^{-1}. The ICP analysis of the electrode after charging to 4.9 V (Table S7) also confirms the removal of approximately one lithium from each formula unit of $\mathrm{Li_2Fe_{1/3}Mn_{1/3}Co_{1/3}P_2O_7}$. When compared against single-component pyrophosphates, the specific capacity of $\mathrm{Li_2Fe_{1/3}Mn_{1/3}Co_{1/3}P_2O_7}$ is a little smaller than that of $\mathrm{Li_2FeP_2O_7}$ (~110 mAh g^{-1})[14] but is larger than those of $\mathrm{Li_2MnP_2O_7}$ (~0 mAh g^{-1})[13] and $\mathrm{Li_2CoP_2O_7}$ (~85 mAh g^{-1}).[12] Importantly, unlike $\mathrm{Li_2Mn_{1-y}Fe_yP_2O_7}$ (<20 mAh g^{-1} for $0 \leq y \leq 0.5$)[13] in which the capacity appears to be severely impaired upon the addition of Mn, the capacity of $\mathrm{Li_2Fe_{1/3}Mn_{1/3}Co_{1/3}P_2O_7}$ suggests that all three TMs are fully active.

Two-Phase vs Single-Phase Reaction. In both the charging and discharging processes, no clear plateaus were observed. Rather, both charging and discharging profiles exhibit sloping curves. This result suggests that $\mathrm{Li_2Fe_{1/3}Mn_{1/3}Co_{1/3}P_2O_7}$ undergoes single-phase reactions during Li insertion and extraction. Both *in situ* and *ex situ* XRD data shown above also support the single-phase reaction consistently. Similarly to the multicomponent olivine case,[21] this phenomenon can be understood by the multicomponent effect. Figure 10 schematically shows the single- vs multicomponent systems that can undergo two-phase and/or single-phase reactions.

A simple electrostatic consideration indicates that the $\mathrm{Li^+}$—$\mathrm{M^{2+}}$ pair is less repulsive (more favorable) than the $\mathrm{Li^+}$—$\mathrm{M^{3+}}$ pair. For the lithium vacancy generated during delithiation, for every vacancy—$\mathrm{M^{2+}}$ pair, there should be an unfavorable $\mathrm{Li^+}$—$\mathrm{M^{3+}}$ pair for charge neutrality. Therefore, the vacancy—$\mathrm{M^{3+}}$ pair can be conveniently thought of as energetically more favorable than the vacancy—$\mathrm{M^{2+}}$ pair.[54,55] For example, for a single-component system M = Fe in Figure 10a, both two- and single-phase reaction intermediates have just $\mathrm{Li^+}$—$\mathrm{Fe^{2+}}$ and vacancy—$\mathrm{Fe^{3+}}$ interactions that are more favorable than the vacancy—$\mathrm{Fe^{2+}}$ and $\mathrm{Li^+}$—$\mathrm{Fe^{3+}}$ pairs. Thus, two- and single-phase pathways are both possible from a simple electrostatic viewpoint. In fact, as indicated from formation energy calculations (Figure S10), $\mathrm{Li_2MnP_2O_7}$ is more likely to undergo a two-phase reaction, whereas $\mathrm{Li_2CoP_2O_7}$ is more likely to have a single-phase reaction.

On the other hand, in a multicomponent system, the TMs with a lower redox potential (Fe) are oxidized first throughout the entire region of the particle. Thus, as in Figure 10b, the Fe/Co multicomponent two-phase reaction, for example, would necessarily yield unfavorable $\mathrm{Li^+}$—$\mathrm{Fe^{3+}}$ pairs in the inner phase and other unfavorable vacancy—$\mathrm{Co^{2+}}$ pairs in the outer phase.

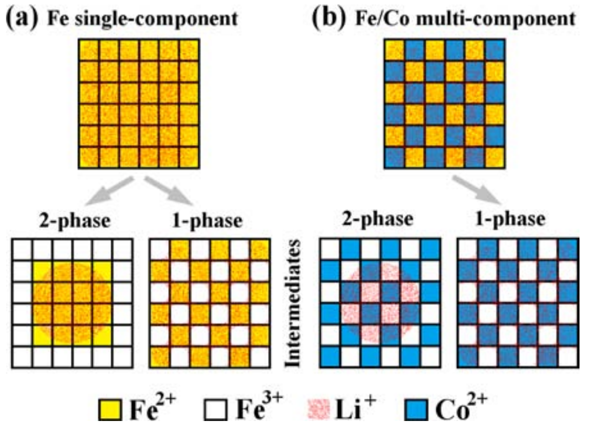

Figure 10. Schematic comparison of 2-phase vs 1-phase reactions for (a) Fe single-component and (b) Fe/Co multicomponent systems. A simple electrostatic consideration suggests that, for a single-component system, 2- and 1-phase reactions are both possible, but for a multicomponent system with homogeneous mixing, a 1-phase reaction is preferred. See the main text for details.

The single-phase reaction, however, generates only favorable interactions, hence preferred in the multicomponent system.

Compared to the olivine case,[21] the potential profile of $Li_2Fe_{1/3}Mn_{1/3}Co_{1/3}P_2O_7$ shows much more vague boundaries between the different TM regions, indicating the enhanced multicomponent effects due to the more uniform mixing of TMs driven by the preferential site occupation.[56] We reveal that the homogeneous mixing of TM and the sequential redox reaction for each TM element with a well-separated potential gap is the underlying physical reason behind the single-phase mode of Li insertion/deinsertion reaction in multicomponent pyrophosphate system. On the basis of these insights, we can predict that, for all multicomponent systems that have a homogeneous mixing and a wide redox gap between different TM elements, the single-phase reaction must be preferred in general.

Activity of Mn. As can be noticed from the QOCP data, the Mn^{2+}/Mn^{3+} redox couple exhibits relatively smaller overpotentials compared to those of other compounds based on the same Mn redox couple. In most cases where Mn^{2+}/Mn^{3+} reacts based on the two-phase reaction, a Jahn−Teller distortion with Mn^{3+} severely deteriorates the mobility of phase boundary and thus the activity of the entire material. Even for the multicomponent olivine case[21] where the compound reacts based on the single-phase reaction, small polaronic conduction of the Mn^{2+}/Mn^{3+} couple resulted in larger overpotentials than other TM redox couples do. While a detailed mechanism for extraordinary low Mn overpotentials observed with the present multicomponent pyrophosphate is currently under further investigation, the favorable Mn occupancy at pyramidal sites causes a more rigorous mixing of Mn with the other TMs in the solid solution because the neighboring octahedral sites should necessarily be occupied by the other two TMs (Table 1) without potential Jahn−Teller distortions. This mixing can be compared with the multicomponent olivine case in which the possibility of Mn to be located in consecutive octahedral sites may not be completely excluded. Moreover, in the present material, Li is first extracted with the oxidation of neighboring Fe sites, leaving a vacancy behind. These vacant sites would help oxidizing Mn^{2+} to Mn^{3+} because of the favorable vacancy−Mn^{3+} interaction described above.[57] This unusual configurational tendency appears to allow for the improved kinetics of the Mn^{2+}/Mn^{3+} couple in this compound.

Asymmetric Potential Behaviors for Fe^{2+}/Fe^{3+} and Co^{2+}/Co^{3+}. Similarly to the multicomponent olivine case,[21] due to the multicomponent solid-solution formation, $Li_2Fe_{1/3}Mn_{1/3}Co_{1/3}P_2O_7$ exhibits higher potentials for the Fe^{2+}/Fe^{3+} redox couple than those of $Li_2FeP_2O_7$ and lower potentials for Co^{2+}/Co^{3+} redox couple than those of $Li_2CoP_2O_7$. However, the degree and trend of the potential shift are different between these two redox couples in both multicomponent compounds. While the multicomponent olivine shows almost the same degree of potential shifts (~0.1 V) for both the upshift of Fe^{2+}/Fe^{3+} and the downshift of Co^{2+}/Co^{3+}, the present multicomponent pyrophosphate shows a significantly larger potential shift for Co^{2+}/Co^{3+} (~0.26 V down) than that for the Fe^{2+}/Fe^{3+} couple (~0.18 V up). Also, in contrast to the multicomponent olivine, during delithiation (Figure 3a), the region for the Fe^{2+}/Fe^{3+} couple exhibits sloping curves, whereas the region for the Co^{2+}/Co^{3+}couple exhibits relatively flat curves. This asymmetric potential behavior between these two TM redox couples is ascribed to the TM configurations in the thermodynamically stable form of $Li_2Fe_{1/3}Mn_{1/3}Co_{1/3}P_2O_7$ as discussed above (Table 1). That is, in the case of Fe, both octahedral and pyramidal sites are energetically favorable, whereas for Co octahedral sites are strongly preferred. Thus, it can be anticipated that the distinct occupancy of the two TMs in the crystal sites gives rise to the asymmetric potential profiles. The site-dependent potential profiles were also supported by the first principles calculations. As shown in Figure 9, for the same TM, the redox potential for the octahedral site is calculated to be lower than that for the pyramidal site, which in conjunction with the Co configuration that occupies mostly octahedral sites results in a more significant potential shift and a relatively flatter curve for the Co^{2+}/Co^{3+} couple. By contrast, the Fe occupancy in both types of sites leads to the sloping profile in the Fe^{2+}/Fe^{3+} region.

Lowering of the Co^{2+}/Co^{3+} Potential. Obviously, the significant downshift of the Co^{2+}/Co^{3+} potential is practically useful because the redox reaction can take place within stable potential windows of most electrolytes. The calculated Co^{2+}/Co^{3+} potential (Figure 9) in our multicomponent compound is even lower than that in $Li_2CoP_2O_7$ for the same octahedral sites. To investigate this additional multicomponent effect on the lowering of the Co^{2+}/Co^{3+} potential, we performed a DFT calculation in a stepwise manner. As shown in Figure 11a, during delithiation, the two Li sites in Figure 1, Li1 and Li4, will be first deintercalated. Both Li sites have one corner sharing and one edge sharing with neighboring pyramidal TM and octahedral TM, respectively. Additionally, because the distance between Li and TM in the octahedral site is shorter, the TMs in octahedral sites are electrostatically more influential on these lithium sites. Therefore, at the intermediate stage (Figure 11b) of the single cobalt compound, $Li_{1.5}CoP_2O_7$, the favorable vacancy−M^{3+}(Oc) interaction (green arrow) is more dominant than the unfavorable vacancy−M^{2+}(Py) interaction. On the contrary, in the multicomponent system, because Fe (or Mn) in the neighboring pyramidal sites is first oxidized, the unfavorable vacancy−M^{2+}(Oc) interaction (red arrow) is more dominant than the favorable vacancy−M^{3+}(Py) interaction. This unfavorable interaction leads to a higher energy intermediate state in the multicomponent system (Figure 11b), equivalent to the lower potential for the Co^{2+}/Co^{3+} redox reaction as shown in

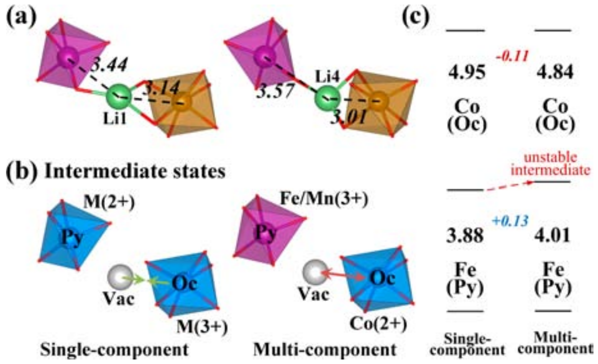

Figure 11. (a) Crystal environments surrounding Li1 and Li4 sites in Figure 1, showing that the TMs in octahedral sites are closer to these lithium sites than those in the pyramidal sites and thus play a more important role electrostatically. Distances are in Å. (b) Due to a particular sequence of oxidation (Oc → Py for sites, Fe → Co for TM elements), the multicomponent Fe/Co system involves an unfavorable vacancy−Co^{2+} interaction in its intermediate state, whereas in the single-component system the intermediate state has a favorable vacancy−-M^{3+} pair. (c) This unstable intermediate state lowers the redox potential of $Co^{2+/3+}$ and raises the potential for $Fe^{2+/3+}$.

Figure 11c. In this context, the intermediate state energy and the redox potential are related on the basis of the fact that the redox potential can be correlated to energy difference between final and initial states.[58] The redox potential of Co^{2+}/Co^{3+} in the Co/Mn pair is also lowered in the same manner as shown in Figure 9. Overall, multicomponent effect on the stability of delithiated intermediates lowers the Co^{2+}/Co^{3+} redox potential substantially compared to that of the single-component Co system.

CONCLUSIONS

(1) Significant improvements in electrochemical and thermal properties for pyrophosphate ($Li_2MP_2O_7$) have been observed in $Li_2Fe_{1/3}Mn_{1/3}Co_{1/3}P_2O_7$ by mixing three TM elements, as compared to single-component analogues as well as the multicomponent olivine.

(2) The underlying origin of the improved battery properties and multicomponent effects in pyrophosphate that distinguishes it from previous related materials is its unique crystal structure where each TM preferentially occupies either an octahedral or pyramidal site specifically.

(3) The favorable energy of homogeneous TM mixing and the sequential redox reaction for each TM element with a sufficient redox gap is the physical reason for the single-phase mode of Li insertion/deinsertion reaction observed in multicomponent pyrophosphate. On the basis of this interpretation, we predict that all multicomponent systems that meet the latter two requirements would undergo the single-phase reaction as a general rule.

(4) The TM mixing raises the Fe^{2+}/Fe^{3+} potential by 0.18 eV to enable a higher energy density and lowers the Co^{2+}/Co^{3+} potential by 0.26 eV for cell operations within the stable electrolyte windows, both of these magnitudes being significantly larger than the 0.1 eV shift observed in the multicomponent olivine case. These extents and asymmetric potential shifts of different TM redox couples are due to the tendency of site-specific TM occupations in pyrophosphate.

(5) The Mn^{2+}/Mn^{3+} redox couple becomes active as a result of the multicomponent effects, similarly to the olivine case, but with a significantly reduced overpotential due to a more rigorous mixing of Mn with other TM elements again driven by the site-specific TM occupations in pyrophosphate.

(6) The single-phase mechanism allows for an extremely small volume change (~0.7%) between the charged and discharged states, suggesting that the multicomponent solid-solution formation contributes to the minimal strain of electrode materials, which is desirable for robust battery performance.

(7) $Li_2Fe_{1/3}Mn_{1/3}Co_{1/3}P_2O_7$ shows exceptionally stable thermal properties, which have not been observed in other multicomponent systems but turn out to be superior to those of other existing cathode materials. The increased thermal stability guarantees the safety for practical applications.

ASSOCIATED CONTENT

Ⓢ Supporting Information

Experimental procedures, details of DFT calculations, FT-IR/ICP-MS data, additional *ex situ* and *in situ* XRD data and their analyses, magnetic momentum/formation energy/mixing energy calculations. This material is available free of charge via the Internet at http://pubs.acs.org.

AUTHOR INFORMATION

Corresponding Author

jangwookchoi@kaist.ac.kr; ysjn@kaist.ac.kr

Author Contributions

¶These authors contributed equally to this work.

Notes

The authors declare no competing financial interest.

ACKNOWLEDGMENTS

We acknowledge the National Research Foundation of Korea Grant funded by the Korean Government (MEST) for the financial support (NRF-2010-0029031, NRF-2012-R1A2A1A01011970, NRF-2010-0023018) and World Class University Program (R-31-2008-000-10055-0). We also thank KISTI supercomputing center for the generous computing time.

REFERENCES

(1) Armand, M.; Tarascon, J. M. *Nature* **2008**, *451*, 652.

(2) Barker, J.; Saidi, M. Y.; Swoyer, J. L. *J. Electrochem. Soc.* **2003**, *150*, A1394.

(3) Barker, J.; Saidi, M. Y.; Swoyer, J. L. *J. Electrochem. Soc.* **2004**, *151*, A1670.

(4) Melot, B. C.; Rousse, G.; Chotard, J. N.; Ati, M.; Rodriguez-Carvajal, J.; Kemei, M. C.; Tarascon, J. M. *Chem. Mater.* **2011**, *23*, 2922.

(5) Barpanda, P.; Ati, M.; Melot, B. C.; Rousse, G.; Chotard, J. N.; Doublet, M. L.; Sougrati, M. T.; Corr, S. A.; Jumas, J. C.; Tarascon, J. M. *Nat. Mater.* **2011**, *10*, 772.

(6) Ati, M.; Sougrati, M. T.; Recham, N.; Barpanda, P.; Leriche, J. B.; Courty, M.; Armand, M.; Jumas, J. C.; Tarascon, J. M. *J. Electrochem. Soc.* **2010**, *157*, A1007.

(7) Barpanda, P.; Recham, N.; Chotard, J. N.; Djellab, K.; Walker, W.; Armand, M.; Tarascon, J. M. *J. Mater. Chem.* **2010**, *20*, 1659.

(8) Tripathi, R.; Gardiner, G. R.; Islam, M. S.; Nazar, L. F. *Chem. Mater.* **2011**, *23*, 2278.

(9) Tripathi, R.; Ramesh, T. N.; Ellis, B. L.; Nazar, L. F. *Angew. Chem.* **2010**, *49*, 8738.

(10) Dong, Y. Z.; Zhao, Y. M.; Fu, P.; Zhou, H.; Hou, X. M. *J. Alloys Compd.* **2008**, *461*, 585.

(11) Yamada, A.; Iwane, N.; Harada, Y.; Nishimura, S.; Koyama, Y.; Tanaka, I. *Adv. Mater.* **2010**, *22*, 3583.

(12) Kim, H.; Lee, S.; Park, Y.-U.; Kim, H.; Kim, J.; Jeon, S.; Kang, K. *Chem. Mater.* **2011**, *23*, 3930.

(13) Zhou, H.; Upreti, S.; Chernova, N. A.; Hautier, G.; Ceder, G.; Whittingham, M. S. *Chem. Mater.* **2010**, *23*, 293.

(14) Nishimura, S.-i.; Nakamura, M.; Natsui, R.; Yamada, A. *J. Am. Chem. Soc.* **2010**, *132*, 13596.

(15) Nishimura, S. I.; Hayase, S.; Kanno, R.; Yashima, M.; Nakayama, N.; Yamada, A. *J. Am. Chem. Soc.* **2008**, *130*, 13212.

(16) Nyten, A.; Abouimrane, A.; Armand, M.; Gustafsson, T.; Thomas, J. O. *Electrochem. Commun.* **2005**, *7*, 156.

(17) Delacourt, C.; Poizot, P.; Tarascon, J.-M.; Masquelier, C. *Nat. Mater.* **2005**, *4*, 254.

(18) Chen, G.; Song, X.; Richardson, T. J. *J. Electrochem. Soc.* **2007**, *154*, A627.

(19) Malik, R.; Zhou, F.; Ceder, G. *Nat. Mater.* **2011**, *10*, 587.

(20) Seo, D. H.; Gwon, H.; Kim, S. W.; Kim, J.; Kang, K. *Chem. Mater.* **2009**, *22*, 518.

(21) Gwon, H.; Seo, D.-H.; Kim, S.-W.; Kim, J.; Kang, K. *Adv. Func. Mater.* **2009**, *19*, 3285.

(22) Gibot, P.; Casas-Cabanas, M.; Laffont, L.; Levasseur, S.; Carlach, P.; Hamelet, S.; Tarascon, J. M.; Masquelier, C. *Nat. Mater.* **2008**, *7*, 741.

(23) Muraliganth, T.; Manthiram, A. *J. Phys. Chem. C* **2010**, *114*, 15530.

(24) Bramnik, N. N.; Bramnik, K. G.; Nikolowski, K.; Hinterstein, M.; Baehtz, C.; Ehrenberg, H. *Electrochem. Solid State Lett.* **2005**, *8*, A379.

(25) Kuo, H. T.; Chan, T. S.; Bagkar, N. C.; Liu, G. Q.; Liu, R. S.; Shen, C. H.; Shy, A. S.; Xing, X. K.; Chen, J. M. *J. Phys. Chem. B* **2008**, *112*, 8017.

(26) Park, Y. U.; Kim, J.; Gwon, H.; Seo, D. H.; Kim, S. W.; Kang, K. *Chem. Mater.* **2010**, *22*, 2573.

(27) Wang, X. J.; Yu, X. Q.; Li, H.; Yang, X. Q.; McBreen, J.; Huang, X. J. *Electrochem. Commun.* **2008**, *10*, 1347.

(28) Barker, J.; Saidi, M. Y. U.S. Patent 7,008,566, 2006.

(29) Zhou, H.; Upreti, S.; Chernova, N. A.; Whittingham, M. S. Abstract 666, International Meeting on Lithium Batteries, Montreal, Canada 2010.

(30) Huang, Q.; Hwu, S.-J. *Inorg. Chem.* **1998**, *37*, 5869.

(31) Bih, H.; Saadoune, I.; Ehrenberg, H.; Fuess, H. *J. Solid State Chem.* **2009**, *182*, 821.

(32) Adam, L.; Guesdon, A.; Raveau, B. *J. Solid State Chem.* **2008**, *181*, 3110.

(33) Rodríguez-Carvajal, J. *Phys. B (Amsterdam, Neth.)* **1993**, *192*, 55.

(34) Padhi, A. K.; Nanjundaswamy, K. S.; Goodenough, J. B. *J. Electrochem. Soc.* **1997**, *144*, 1188.

(35) Meethong, N.; Huang, H.-Y. S.; Speakman, S. a.; Carter, W. C.; Chiang, Y.-M. *Adv. Func. Mater.* **2007**, *17*, 1115.

(36) Berg, H.; Thomas, J. O. *Solid State Ionics* **1999**, *126*, 227.

(37) Yamada, A.; Koizumi, H.; Nishimura, S. I.; Sonoyama, N.; Kanno, R.; Yonemura, M.; Nakamura, T.; Kobayashi, Y. *Nat. Mater.* **2006**, *5*, 357.

(38) Huang, H.; Faulkner, T.; Barker, J.; Saidi, M. *J. Power Sources* **2009**, *189*, 748.

(39) Yamada, A.; Kudo, Y.; Liu, K. Y. *J. Electrochem. Soc.* **2001**, *148*, A747.

(40) Kim, S.-W.; Kim, J.; Gwon, H.; Kang, K. *J. Electrochem. Soc.* **2009**, *156*, A635.

(41) Dodd, J. L.; Yazami, R.; Fultz, B. *Electrochem. Solid State Lett.* **2006**, *9*, A151.

(42) Ong, S. P.; Jain, A.; Hautier, G.; Kang, B.; Ceder, G. *Electrochem. Commun.* **2010**, *12*, 427.

(43) Furushima, Y.; Yanagisawa, C.; Nakagawa, T.; Aoki, Y.; Muraki, N. *J. Power Sources* **2011**, *196*, 2260.

(44) Kresse, G. *Comput. Mater. Sci.* **1996**, *6*, 15.

(45) Blöchl, P. E. *Phys. Rev. B* **1994**, *50*, 17953.

(46) Perdew, J. P.; Burke, K.; Ernzerhof, M. *Phys. Rev. Lett.* **1996**, *77*, 3865.

(47) Dudarev, S. L.; Botton, G. A.; Savrasov, S. Y.; Humphreys, C. J.; Sutton, A. P. *Phys. Rev. B* **1998**, *57*, 1505.

(48) Jain, A.; Hautier, G.; Moore, C. J.; Ping Ong, S.; Fischer, C. C.; Mueller, T.; Persson, K. a.; Ceder, G. *Comput. Mater. Sci.* **2011**, *50*, 2295.

(49) Wang, L.; Maxisch, T.; Ceder, G. *Phys. Rev. B* **2006**, *73*, 195107.

(50) Momma, K.; Izumi, F. *J. Appl. Crystallogr.* **2008**, *41*, 653.

(51) Monkhorst, H. J. *Phys. Rev. B* **1976**, *13*, 5188.

(52) Toukmaji, A. *Comput. Phys. Sci.* **1996**, *95*, 73.

(53) Hautier, G.; Jain, A.; Ong, S. P.; Kang, B.; Moore, C.; Doe, R.; Ceder, G. *Chem. Mater.* **2011**, 3495.

(54) Zhou, F.; Maxisch, T.; Ceder, G. *Phys. Rev. Lett.* **2006**, *97*, 1.

(55) Malik, R.; Zhou, F.; Ceder, G. *Phys. Rev. B* **2009**, *79*, 1.

(56) Kim, H.; Seo, D.-H.; Kim, H.; Park, I.; Hong, J.; Park, K.-Y.; Kang, K. *Chem. Mater.* **2012**, *24*, 720.

(57) Kim, J.; Seo, D. H.; Kim, S. W.; Park, Y. U.; Kang, K. *Chem. Commun.* **2010**, *46*, 1305.

(58) Aydinol, M.; Kohan, A.; Ceder, G.; Cho, K.; Joannopoulos, J. *Phys. Rev. B* **1997**, *56*, 1354.